A Risk-Averse Conic Model for Networked Microgrids Planning With Reconfiguration and Reorganizations

Xiaoyu Cao, Jianxue Wang, *Senior Member, IEEE*, Jianhui Wang, *Senior Member, IEEE*, and Bo Zeng, *Member, IEEE*

***Abstract*—The advanced switching techniques enable the topology reconfiguration of microgrids (MGs) in active distribution network. In this paper, we enhance and generalize the traditional reconfiguration strategy resorting to the concept of "dynamic MGs" (i.e., the reorganization of MGs boundaries), to achieve a higher operational feasibility against the emergency islandings. Also, a risk-averse two-stage mixed integer conic program model is presented to support the networked MGs planning with generalized reconfiguration decisions. The MGs capacity expansion and seasonal reconfiguration decisions are made in the first stage, and validated under stochastic islanding scenarios in the second stage, where the network operations are captured by a second-order conic program (SOCP). Furthermore, a conditional value-at-risk (CVaR) measure is involved to quantitatively control the islanding risks. By theoretically proving the strong duality of the SOCP subproblem, we develop and customize Benders decomposition method with the guaranteed finite convergence to the optimal value. Finally, numerical results on 33- and 56-bus networked MGs validate the effectiveness of proposed reconfiguration strategy as well as planning approach. Our method demonstrates a cost-saving up to 22.56% when comparing to the traditional scheme with fixed MGs boundaries.**

***Index Terms*—Microgrids expansion planning, generalized network reconfiguration, stochastic mixed-integer conic program, condition value-at-risk, Benders decomposition.**

Manuscript received September 15, 2018; revised January 5, 2019 and April 17, 2019; accepted July 7, 2019. Date of publication July 10, 2019; date of current version December 23, 2019. This work was supported in part by the Key Research and Development Program of Shaanxi through "Research and Demonstration on Key Technologies of Energy Internet Planning and Operation Based on Multi-Time Scale and Multi-Energy Complementary Optimization" under Grant 2019ZDLGY18-01. The work of B. Zeng was supported in part by the National Science Foundation under Grant CMMI 1635472, and in part by DoE under Grant OE0000842. Paper no. TSG-01356-2018. *(Corresponding author: Jianxue Wang.)*

X. Cao is with Xi'an Jiaotong University, Xi'an 710049, China (e-mail: cxykeven2019@mail.xjtu.edu.cn).

J. Wang is with the School of Electrical Engineering, Xi'an Jiaotong University, Xi'an 710049, China, and also with the Shaanxi Key Laboratory of Smart Grid, Xi'an Jiaotong University, Xi'an 710049, China (e-mail: jxwang@mail.xjtu.edu.cn).

J. Wang is with the Department of Electrical and Computer Engineering, Southern Methodist University, Dallas, TX 75275 USA (e-mail: jianhui@smu.edu).

B. Zeng is with the Department of Industrial Engineering, University of Pittsburgh, Pittsburgh, PA 15106 USA, and also with the Department of Electrical and Computer Engineering, University of Pittsburgh, Pittsburgh, PA 15106 USA (e-mail: bzeng@pitt.edu).

Color versions of one or more of the figures in this paper are available online at http://ieeexplore.ieee.org.

Digital Object Identifier 10.1109/TSG.2019.2927833

NOMENCLATURE

Set and Index

(t, h)	Time index of hour h in season t
$\mathcal{E}/(i, j)$	Set/index of branches
$\mathcal{M}$	Set of microgrids
$\mathcal{N}/i$	Set/index of nodes
Ω/ω	Set/index of stochastic scenarios
Ψ	Set of nodes with existing DER installation
H/h	Set/index of hours
k	Index of candidate DERs
T/t	Set/index of seasons.

Parameters

$\bar{C}^0_{k,i}$	Existing power capacity of DER k at node i
$\bar{E}^0_{k,i}$	Existing energy capacity of ES k at node i
$\delta r^{t,h}_{k,i}(\omega)$, $\delta l^{t,h}_i(\omega)$	Capacity factor of RES k/load demand (under scenario ω) at node i in (t, h)
Δ_h	Time slot of microgrids operation
η_k	Charge/discharge efficiency of ES k
$\hbar^t$	Scaling factor from typical day to season t
λ^{ec}_k	Operating cost coefficient of ES k
λ^{fc}_k	Fuel cost coefficient of DFG k
λ^{om}_k	Fixed maintenance cost coefficient of DER k
μ_k	Maximum depth of discharge (DOD) of ES k
$\bar{I}$	Upper bound of current magnitudes
$\bar{p}_0, \bar{q}_0$	Active/reactive power limits of substation
$\bar{S}^{\text{p}}, \bar{S}^{\text{q}}$	Upper limits of active/reactive power flows
$\phi^{\text{ec}}_k, \phi^{\text{pc}}_k$	Annualized unit energy/power cost of ES k
ϕ^{ic}_k	Annualized unit cost of RES or DFG k
π_ω	Occurrence probability of scenario ω
$\tilde{\delta} r^{t,h}_{k,i}, \tilde{\delta} l^{t,h}_i$	Capacity factor of RES k/load demand (under an average scenario) at node i in (t, h)
$\underline{U}, \bar{U}$	Allowable range of voltage magnitudes
φ	Penalty cost factor of RES curtailment
ϑ	Cost coefficient of power loss
ξ	Penalty cost factor of load shedding
Dp^t_i, Dq^t_i	Active/reactive load capacity at node i in season t
r_{ij}, x_{ij}	Resistance/reactance of branch (i, j)
$ru^{t,h}_i$	Operating reserve requirement at node i in (t, h)
sc^0_i	Installed capacity of shunt capacitors at node i
U_0	Reference voltage level.

Variables

$\bar{C}_{k,i}$	Newly-added power capacity of DER k at node i
$\bar{E}_{k,i}$	Newly-added energy capacity of ES k at node i
$\Delta v_{ij}^{t,h}$	Variables to control the enforcement state of KVL constraints on branch (i,j) in (t,h)
$d_{k,i}^{t,h}, c_{k,i}^{t,h}$	Discharge/charge power of ES k at node i in (t,h)
$e_{k,i}^{t,h}$	Stored energy of ES k at node i in (t,h)
fp_{ij}^{t}, fq_{ij}^{t}	Virtual active/reactive power flows on branch (i,j) in season t
$g_{k,i}^{t,h}, q_{k,i}^{t,h}$	Active/reactive output of DER k at node i in (t,h)
$gl_{i}^{t,h}$	Renewable energy curtailment at node i in (t,h)
Gp_i, Gq_i	Active/reactive power capacity at node i
$p_0^{t,h}, q_0^{t,h}$	Exchanged power at substation node in (t,h)
$P_{ij}^{t,h}, Q_{ij}^{t,h}$	Active/reactive flows on branch (i,j) in (t,h)
$pl_i^{t,h}, ql_i^{t,h}$	Active/reactive load shedding at node i in (t,h)
u_{ij}^{t}	Binary variable to indicate the open/closed status of branch (i,j) in season t
$v_i^{t,h}, \ell_{ij}^{t,h}$	Squared magnitudes of voltage and current in (t,h)
w_{ij}^{t}	Binary variable to indicate the placement of PCC on branch (i,j) in season t.

I. Introduction

THE MICROGRIDS are considered as the essential building blocks of the active distribution networks (ADN) [1]. Several neighboring microgrids with distributed energy resources (DERs) can be networked to achieve higher system performance, e.g., energy efficiency, reliability, and resilience [2], [3]. In case of extreme events (e.g., utility blackouts or natural disasters), particularly, the microgrids can be operated as self-adequacy islands to preserve the critical loads and to assist the service restoration of adjacent areas, which thus makes a highly reliable and "self-healing" system [2].

To realize the islanding functionality, it requires the microgrids to be properly configured with adequate DER resources and reliable network topology. Hence, the planning issues of networked microgrids, especially the initial design of network layout and DERs integration, have been extensively discussed in the current literatures, e.g., [4]–[9]. As indicated by [10], [11], however, the static planning strategy could hardly capture the dynamic changes in system conditions (e.g., demand growth, seasonal rhythms of wind or solar resources, fuel price fluctuation) under the long-term timescale. In addition to the capital investment, the microgrids infrastructure should be reinforced periodically to maintain its operational feasibility. One typical way to harden the microgrids is resorting to the capacity expansion of DERs, which has been well modeled and numerically verified in several recent publications, e.g., [10]–[17]. Reference [10] presented a stochastic program method to optimize the capacity expansion of microgrids considering the randomness of DERs output. Reference [11] proposed a chance constrained information-gap decision model to handle both the random factors (e.g., variable DERs generation and load profile) and nonrandom uncertainties (e.g., demand growth) in multi-stage microgrids expansion planning. Reference [12] designed a tri-level microgrids planning framework to coordinate the demand expansion with resource configuration and operational optimization under load uncertainties. In [13], the microgrids expansion planning was studied with comprehensive modeling of battery energy storage. In [14], [15], the capacity expansion of DERs was optimized under uncertain demand and DERs output, along with the partitioning of distribution network into several interconnected microgrids. Reference [16] developed a multi-stage and multi-load-scenario formulation to deal with the expansion planning of ADN and DERs capacity considering the operation strategies of microgrids. Similarly, the distribution network expansion and microgrids deployment were co-optimized through a bi-level approach in [17].

Certainly, the reinforcement of microgrids can be achieved through network expansion as in [16], [17]. Nevertheless, we mention that the target of microgrids deployment is usually to defer the upgrades of distribution facilities. So, instead of the network expansion, a more practical strategy is to reconfigure the existing microgrids [1] by changing the open/closed status of remotely-controlled smart switches (SSWs). The concept of network reconfiguration is originally adopted in distribution system for the purposes such as power loss reduction, congestion management, voltage violation mitigation, and DERs hostility improvement [18]–[25]. Analogously, the reconfiguration strategy is also applicable to the microgrids in ADN. Reference [26] presented a microgrid reconfiguration (MRC) decision model to minimize the total cost of transmission loss and switching actions. In [27], the MRC was modeled as a reliability-oriented chance constrained program and solved through a sampling-based convex relaxation. Reference [28] developed a multi-objective framework for the reconfiguration of islanded microgrids to seek for Pareto-optimality between load survivability and cost-benefits. Reference [29], [30] studied the dynamic reconfiguration of microgrid considering the cost-minimization under grid-connected operation as well as the reliability enhancement for islanding. Reference [31] implemented a real-time MRC algorithm to isolate the contingency regions in case of natural disasters.

We notice that the aforementioned network reconfiguration strategies are all implemented under the traditional concept of microgrid, i.e., with clearly-defined and fixed boundaries [32]. Note that the networking supports the sharing of critical DER resources among microgrids. Once the networking is damaged (e.g., under natural disasters), however, the fixed boundaries may lead to severe demand-supply unbalance within some of the isolated microgrids. To fit the dynamic system conditions and prepare for emergency islandings, it requires for a more flexible topology control scheme, where the energy resources can be proactively relocated to gain higher operational feasibility. Hence, we generalize the traditional reconfiguration strategy (with static microgrids boundaries) by using the new concept of "dynamic microgrids" [33], [34], i.e., the flexible reorganization of microgrids boundaries, so as to ensure the self-adequacy of networked microgrids under extreme events. We mention that the generalized reconfiguration strategy with reorganizable boundaries is abbreviated as *G-MRC*.

Also, this paper develops a risk-averse two-stage mixed integer conic program formulation to support the microgrids

expansion planning with generalized reconfiguration decisions. Note that a two-stage planning framework is designed to represent the functionality of G-MRC under normal operation and emergency islandings respectively. The first-stage problem is to co-optimize the microgrids capacity expansion and generalized reconfiguration decisions, along with the grid-connected scheduling of microgrids. Aided by advanced switching and EMS techniques, the microgrids in ADN can be reconfigured and reorganized periodically to capture the varying system conditions under different timescales, e.g., yearly, seasonally, or monthly. In this study, the microgrids are assumed to be reconfigured under a seasonal basis, which is practically reasonable for a long-term planning problem. Then, in the second-stage, a *minimum energy loss model* is defined under the seasonal stochastic scenarios (representing the variability of DERs' generation and load demand) to validate the first-stage decisions given the islanding of on-emergency microgrids. Note that in both planning stages, the detailed operations of reconfigurable network can be described by an accurate AC power flow model with convexified SOCP formulation. Furthermore, our planning formulation incorporates a CVaR measure to hedge against the operational risks of those very adversarial islanding scenarios.

In addition, the modeling of G-MRC will introduce a large number of binary variables to our planning formulation. Together with the AC power flow structure for every stochastic scenario, the resultant mixed integer SOCP model could be computationally intractable even using state-of-the-art commercial solvers (e.g., CPLEX). By proving the strong duality of the SOCP subproblem, we develop and customize a Benders decomposition method that converges to the optimal value in finite steps. Indeed, we drastically relieves the computational burden of the proposed planning formulation. Hence, comparing to many published results, we note that the presented mixed integer SOCP model with CVaR consideration generalizes conventional optimization models for MRC (e.g., [27], [29], [30]), and the algorithm development theoretically strengthens the existing computational methods (e.g., [35], [36]). Next, we summarize our main contributions:

1) A generalized MRC strategy with dynamic boundaries is presented, which is analytically supported and demonstrated by a reorganizable microgrids planning (RMP) model formulated as a two-stage stochastic program with a CVaR measure. In particular, the G-MRC operations are accurately captured by a mixed integer and SOCP-based power flow model.
2) The strong duality of our conic G-MRC model is theoretically proved, which supports the customization of Benders decomposition algorithm to exactly and efficiently solve the proposed mixed integer conic planning formulation.
3) Our numerical results reveal that a significant benefit of G-MRC (i.e., *the cost saving over 22.56% for a real-world system*) comparing to the traditional network reconfiguration with fixed boundaries, which validates the effectiveness of the proposed strategy in practice.

The remainder of this paper is organized as below. Section II outlines the generalized reconfiguration strategy. Section III formulates the CVaR-based stochastic conic program model for reorganizable microgrids planning. Section IV presents the strong-conic-duality based Benders decomposition algorithm. The proposed method is numerically verified in Section V. Finally, conclusions are drawn in Section VI.

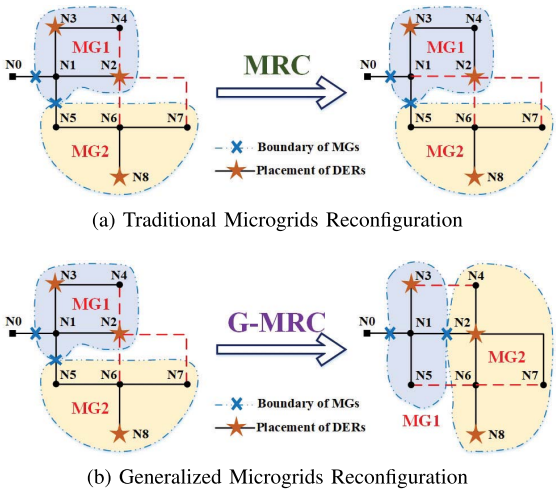

(a) Traditional Microgrids Reconfiguration

(b) Generalized Microgrids Reconfiguration

Fig. 1. Traditional MRC vs. G-MRC.

II. Generalized Microgrids Reconfiguration With Reorganizable Boundaries

A. Definition

As mentioned in [26]–[31], the network reconfiguration is usually conducted to improve the operational feasibility (e.g., power loss reduction, voltage regulation) of a microgrid. For a cluster of networked and interdependent microgrids, however, the freedom of reconfiguration could be restricted by their fixed inner boundaries, and thus may not fit well. As demonstrated in Fig. 1(a), for example, the reconfiguration of MG1 can be conducted by closing the tie SSW at line L2-4 while opening the sectionalizing SSW at L1-2 (or L1-3, L3-4). But it is not allowed to close the tie SSW at L2-6 or L2-7 since they are out of the coverage area of MG1. To enable the topology control with higher flexibility and a broader scope, we combine the traditional MRC strategy with a new paradigm of networked microgrids that holds dynamic and reorganizable boundaries. Following the existing concept, the **generalized microgrids reconfiguration (G-MRC)** can be defined as "a network refinement strategy that changes not only the topology but also the inner boundaries (and thus the resource re-allocation over flexibly scaling subsystems) among a cluster of networked and interdependent microgrids".

Note that we relax the assumption of fixed boundaries so that the scale and feeder configuration of each microgrid can both be flexibly adjusted, along with the proactive re-allocation of critical DER resources among microgrids. As shown in Fig. 1(b), the boundary (i.e., PCC point) between MG1 and MG2 is switched from L1-5 to L1-2, which thus results in a shrunken MG1 and an expanded MG2. Consequently, the DERs installed at node N2 is transferred out of MG1, and instead, to supply the load nods in MG2. Moreover, without the boundary restrictions, the freedom of reconfiguration

extends from each single microgrid to the entire networked system.

B. Motivation

Based on Fig. 1, we note that G-MRC serves as a preventive strategy to support the network reinforcement of microgrids, specifically for extreme events (e.g., utility blackouts or natural disasters). In such cases, the networked system has to separate from the main grid and split apart into several islanded microgrids. To ensure the power balance of each single entity, a de-energized microgrid (e.g., MG2 in Fig. 1) could be reinforced by receiving the DER nodes from (or transferring the load nodes to) those over-adequacy microgrids (e.g., MG1 in Fig. 1) through preventive G-MRC operations. Thus, the co-optimization of topology reconfiguration and dynamic boundaries enables an improved immunity against the energy loss risks brought by emergency islandings. We mention that a great benefit of networking is to gain additional reserves for on-emergency microgrids typically through their interconnection and thus the sharing of critical DER resources. Aided by G-MRC, this benefit can also be achieved through the proactive re-allocation of DER resources, which thus improves the reliability and operational flexibility of islanded microgrids as well as the cost-efficiency of facility investment.

C. Analytical Modeling

The operations of G-MRC are modeled on an ADN that hosts several interconnected microgrids. Without loss of generality, our method is applied to the networked microgrids with a spanning-tree structure, which is represented by $(\mathcal{N}, \mathcal{E}, \mathcal{M})$. Let $\mathcal{N}$ denote the set of nodes where the unique root node (i.e., substation) is indexed by 0 and the rest nodes are indexed by $i = 1, 2, \ldots, n \in \mathcal{N}^+$. Let $\mathcal{E}$ denote the set of branches, which are indexed by $(i, j) \in \mathcal{E}$. Let $\mathcal{M}$ denote the set of microgrids, which can be considered as subgraphs of $(\mathcal{N}, \mathcal{E})$.

Accordingly, we introduce two sets of binary variables, i.e., u_{ij}^t and w_{ij}^t, to represent the G-MRC decisions (as in Fig. 1(b)). Note that u_{ij}^t is to control the feeder configuration by closing the (originally opened) tie SSWs ($u_{ij}^t \coloneqq 0 \to 1$) while opening the (originally closed) sectionalizing SSWs ($u_{ij}^t \coloneqq 1 \to 0$). Moreover, w_{ij}^t is to control the reorganization of microgrids boundaries, which depends on the placement of PCC points. Note that $w_{ij}^t = 1$ indicates that a PCC is placed on branch (i, j) and vice versa. Clearly, we have

$$w_{ij}^t \le u_{ij}^t, \quad \forall (i,j) \in \mathcal{E}, \forall t \in T \tag{1}$$

Accordingly, the G-MRC actions can be analytically expressed as the changing status of binary variables u_{ij}^t and w_{ij}^t. The total number of changed binary status (i.e., ON/OFF status of SSWs) in each season should be limited as:

$$\sum_{(i,j)\in\mathcal{E}} |u_{ij}^t - u_{ij}^{t-1}| \le N_{\mathrm{nr}}^t, \quad \forall t \in T \tag{2}$$

$$\sum_{(i,j)\in\mathcal{E}} |w_{ij}^t - w_{ij}^{t-1}| \le N_{\mathrm{pr}}^t, \quad \forall t \in T \tag{3}$$

where N_{nr}^t and N_{pr}^t define the number limits of G-MRC actions in season t, while the tuple (u_{ij}^0, w_{ij}^0) represents the initial topology of networked microgrids. In addition to (2) and (3), it also requires the reconfigured network to hold a spanning-tree topology as in (4)-(7) [22]–[24].

$$\sum_{(i,j)\in\mathcal{E}} u_{ij}^t = |\mathcal{N}| - 1, \quad \forall t \in T \tag{4}$$

$$\sum_{j\in\Gamma(i)} \varrho_{ij}^t = -1, \quad \forall i \in \mathcal{N}^+, \forall t \in T \tag{5}$$

$$-\overline{S}_{ij} u_{ij}^t \le \varrho_{ij}^t \le \overline{S}_{ij} u_{ij}^t, \quad \forall (i,j) \in \mathcal{E}, \forall t \in T \tag{6}$$

$$\sum_{j\in\Gamma(0)} \varrho_{ij}^t = \kappa_0^t, \quad \forall t \in T \tag{7}$$

where $|\mathcal{N}|$ denotes the cardinality of node set. Note that in (4), the number of branches with closed switches is required to be equal to the number of non-root nodes. Also, a group of virtual power balance constraints, i.e., (5)-(7), are imposed to ensure the network connectivity. We note that (5) enforces the power balance requirement for node $i \in \mathcal{N}^+$ subject to fictitious unit load (1 p.u.), where $\Gamma(i)$ is the set of nodes that connect to node i. The virtual load flow ϱ_{ij}^t is nonzero only on the connected branches as in (6), where $\overline{S}_{ij}$ is the power flow limit on branch (i, j). Besides, as in (7), the fictitious load in reconfigured system can only be fed through the substation node by fictitious inflow κ_0^t. As mentioned in [22]–[24], the enforcement of constraints (4)-(7) necessarily guarantees the radiality and connectivity of the entire reconfigured network.

Furthermore, when encountering the extreme events, the SSWs at substation and PCCs will be opened ($w_{ij} \coloneqq 1 \to 0$) to separate the on-emergency microgrids as electrical islands. In such cases, we use $u_{ij} - w_{ij}$ instead of u_{ij} to indicate the ON/OFF status of line switches. To ensure the radiality of the partitioned network, (4)-(7) are extended to derive a group of *self-energized subtree* constraints as in (8)-(12).

$$\sum_{(i,j)\in\mathcal{E}} \left(u_{ij}^t - w_{ij}^t\right) = |\mathcal{N}| - |\mathcal{M}|, \quad \forall t \in T \tag{8}$$

$$\sum_{j\in\Gamma(i)} fp_{ij}^t \le Gp_i - Dp_i^t, \quad \forall i \in \mathcal{N}^+, \forall t \in T \tag{9}$$

$$\sum_{j\in\Gamma(i)} fq_{ij}^t \le Gq_i - Dq_i^t, \quad \forall i \in \mathcal{N}^+, \forall t \in T \tag{10}$$

$$\overline{S}_{ij}^{\mathrm{p}}\left(w_{ij}^t - u_{ij}^t\right) \le fp_{ij}^t \le \overline{S}_{ij}^{\mathrm{p}}\left(u_{ij}^t - w_{ij}^t\right), \forall (i,j) \in \mathcal{E}, \forall t \in T \tag{11}$$

$$\overline{S}_{ij}^{\mathrm{q}}\left(w_{ij}^t - u_{ij}^t\right) \le fq_{ij}^t \le \overline{S}_{ij}^{\mathrm{q}}\left(u_{ij}^t - w_{ij}^t\right), \forall (i,j) \in \mathcal{E}, \forall t \in T \tag{12}$$

where $|\mathcal{M}|$ denotes the cardinality of microgrid set. Note that (8) is to partition the original spanning-tree graph into $|\mathcal{M}|$ subtrees (i.e., microgrids). In analogy to (5)-(7), we develop constraints (9)-(12) to enforce the connectivity and radiality on each subtree. Moreover, the capacity balance constraints are introduced as in (9) and (10) [11] to guarantee that the nodal load capacity is overly satisfied (with reserve margins) so that every subtree can be self-energized.

TABLE I
DIFFERENCES BETWEEN TRADITIONAL MRC AND GENERALIZED MRC

Items	Traditional MRC	**Generalized MRC**
Definition	Reconfigure the distribution feeders by changing the open/closed status of line switches in microgrids	Refine both the topology and inner boundaries to adjust the coverage areas, feeder configuration, and DERs allocation of networked microgrids
Motivation	To improve the operational feasibility (e.g., power loss reduction, voltage regulation) of grid-connected microgids	To reinforce the networked microgrids as a preventive strategy for emergency islandings, as well as a regular way to enhance the system performance under grid-connected operation
Flexibility	With the restriction of fixed boundaries	With dynamically reorganizable boundaries

D. Differences of Generalized MRC and Traditional MRC

In the following, we highlight the major differences of G-MRC from the existing MRC strategy (as in [26]–[31]):

1) *On the Definitions:* The traditional MRC only permits limited refinements on the topology subject to clearly-defined territory of microgrids. Differently, the generalized MRC changes both the topology and inner boundaries, which leads to adjustable coverage areas, feeder reconfiguration, and DERs re-allocation of networked microgrids.
2) *On the Motivations:* The target of MRC is generally to improve the operational performance of grid-connected microgrids. However, it could not remedy the demand-supply unbalances under islanded operation. Differently, the major concern of G-MRC is to reinforce the microgrids with adequate self-energizing capacity for emergency islandings. Also, it preserves the normal reconfiguration functionality when applying to the grid-connected operations.
3) *On the Flexibility:* The MRC is conducted with the restriction of fixed microgrids boundaries. In contrast, G-MRC provides a much higher flexibility to dynamically and adaptively reorganize the microgrids boundaries.

Finally, the aforementioned comparisons are summarized as in Table I.

III. CVaR-Based Two-Stage Formulation for Reconfigurable Microgrids Planning

A. 1st-Stage Problem: Co-Optimization of Generalized Microgrids Reconfiguration and Capacity Expansion Planning

1) Objective Function: The first-stage objective is to minimize the investment cost of microgrids expansion (z_{inv}) and the grid-connected operational cost (z_{goc}) before the realization of uncertainties, which can be written as follows:

$$\min \ z_{\text{inv}} + z_{\text{goc}} \tag{13}$$

$$z_{\text{inv}} = \sum_{i\in\Psi}\left[\sum_{k\in\{\text{res,dfg}\}} \phi_k^{\text{ic}}\bar{C}_{k,i} + \sum_{k\in\ \text{es}}\left(\phi_k^{\text{ec}}\bar{E}_{k,i} + \phi_k^{\text{pc}}\bar{C}_{k,i}\right)\right] \tag{14}$$

$$\begin{aligned} z_{\text{goc}} = &\sum_{i\in\Psi}\sum_{k\in\{\text{res,dfg,es}\}} \lambda_k^{\text{om}}\bar{C}_{k,i} + \sum_{t\in T}\sum_{h\in H}\sum_{i\in\Psi}\sum_{k\in\text{dfg}} \hbar^t\lambda_k^{\text{fc}} g_{k,i}^{t,h}\Delta_h \\ &+ \sum_{t\in T}\sum_{h\in H}\sum_{i\in\Psi}\sum_{k\in\text{es}} \hbar^t\frac{\lambda_k^{\text{ec}}}{2}\left(d_{k,i}^{t,h} + c_{k,i}^{t,h}\right)\Delta_h \\ &+ \sum_{t\in T}\sum_{h\in H}\hbar^t\left(\rho^h p_0^{t,h}\Delta_h + \sum_{(i,j)\in\mathcal{E}}\vartheta r_{ij}\ell_{ij}^{t,h}\Delta_h\right) \end{aligned} \tag{15}$$

As shown in (14), the investment cost of newly-added DERs is evaluated on a yearly basis. Without loss of generality, the capacity expansion (i.e., discrete decisions with a resolution of 1kW/1kWh) is conducted on a specified nodes set with existing DER installation, and the candidate DER types include renewable energy sources (RES), dispatchable fuel generators (DFG), and energy storage devices (ES) [11]. The operational cost in (15) is comprised of the fixed maintenance cost, the fuel cost of DFGs, the operating cost of ES, the power bargain cost between microgrids and utility grid, and the network loss cost. Note that typical days are sampled to represent the seasonal operation of microgrids, where Δ_h denotes the time slot. All these daily cost terms are then scaled to derive the seasonal values by a factor $\hbar^t$.

2) Investment Constraints:

$$0 \le \bar{C}_{k,i} \le C_{k,i}^{\max}, \quad \forall k \in \{\text{res,dfg,es}\}, \forall i \in \Psi \tag{16}$$

$$\beta_k^{\min}\bar{C}_{k,i} \le \bar{E}_{k,i} \le \beta_k^{\max}\bar{C}_{k,i}, \quad \forall k \in \text{es}, \forall i \in \Psi \tag{17}$$

$$Gp_i = \begin{cases} \sum_{k\in\{\text{res,dfg,es}\}}\left(\bar{C}_{k,i} + \bar{C}_{k,i}^0\right), & \forall i \in \Psi \\ 0, & \forall i \in \mathcal{N}^+/\Psi \end{cases} \tag{18}$$

$$Gq_i = \begin{cases} sc_i^0 + \sum_{k\in\text{res}}\gamma_k^{\max}\left(\bar{C}_{k,i} + \bar{C}_{k,i}^0\right), & \forall i \in \Psi \\ sc_i^0, & \forall i \in \mathcal{N}^+/\Psi \end{cases} \tag{19}$$

Note that the power capacity expansion of DERs is constrained by (16). Particularly, the power capacity of newly-added ES is used to scale its energy capacity through factors $\beta_k^{\max} \ge \beta_k^{\min} \ge 1$ as in (17). The active/reactive components of nodal power capacity are defined in (18) and (19) respectively.

3) Operational Constraints: Note that in our first-stage problem, a set of average operating scenarios (under different seasons) are included to support the seasonal G-MRC decisions, which are constrained as in (20)-(39).

$$p_{g,i}^{t,h} = \begin{cases} \sum_{k\in\{\text{res,dfg}\}} g_{k,i}^{t,h} + \sum_{k\in\text{es}}\left(d_{k,i}^{t,h} - c_{k,i}^{t,h}\right), & \forall i \in \Psi, \forall t, \forall h \\ 0, & \forall i \in \mathcal{N}^+/\Psi, \forall t, \forall h \end{cases} \tag{20}$$

$$q_{g,i}^{t,h} = \begin{cases} sc_i^0 + \sum_{k\in\text{res}} q_{k,i}^{t,h}, & \forall i \in \Psi, \forall t, \forall h \\ sc_i^0, & \forall i \in \mathcal{N}^+/\Psi, \forall t, \forall h \end{cases} \tag{21}$$

$$g_{k,i}^{t,h} = \tilde{\delta} r_{k,i}^{t,h}\left(\bar{C}_{k,i} + \bar{C}_{k,i}^0\right), \quad \forall k \in \text{res}, \forall i \in \Psi, \forall t, \forall h \tag{22}$$

$$\gamma_k^{\min} g_{k,i}^{t,h} \le q_{k,i}^{t,h} \le \gamma_k^{\max} g_{k,i}^{t,h}, \quad \forall k \in \text{res}, \forall i \in \Psi, \forall t, \forall h \tag{23}$$

$$0 \le g_{k,i}^{t,h} \le \bar{C}_{k,i} + \bar{C}_{k,i}^0, \quad \forall k \in \text{dfg}, \forall i \in \Psi, \forall t, \forall h \tag{24}$$

$$\sum_{k\in\text{dfg}}\left(\bar{C}_{k,i} + \bar{C}_{k,i}^0 - g_{k,i}^{t,h}\right) \ge r u_i^{t,h}, \quad \forall i \in \Psi, \forall t, \forall h \tag{25}$$

$$0 \le c_{k,i}^{t,h}, d_{k,i}^{t,h} \le \bar{C}_{k,i} + \bar{C}_{k,i}^0, \quad \forall k \in \text{es}, \forall i \in \Psi, \forall t, \forall h \tag{26}$$

$$e_{k,i}^{t,h+1} = e_{k,i}^{t,h} + \eta_k c_{k,i}^{t,h} - d_{k,i}^{t,h}/\eta_k, \ \forall k \in \text{es}, \forall i \in \Psi, \forall t, \forall h \tag{27}$$

$$\mu_k\left(\bar{E}_{k,i} + \bar{E}_{k,i}^0\right) \le e_{k,i}^{t,h} \le \bar{E}_{k,i} + \bar{E}_{k,i}^0, \forall k \in \text{es}, \forall i, \forall t, \forall h \tag{28}$$

$$e_{k,i}^{t,0} = e_{k,i}^{t,H}, \quad \forall k \in \text{es}, \forall i \in \Psi, \forall t, \forall h \tag{29}$$

$$p_{g,i}^{t,h} - \tilde{\delta} l_i^{t,h} D p_i^t = \sum_{j\in\Theta(i)} P_{ij}^{t,h} - \left(P_{mi}^{t,h} - r_{mi}\ell_{mi}^{t,h}\right), \quad \forall i \in \mathcal{N}^+, \forall t, \forall h \tag{30}$$

$$q_{g,i}^{t,h} - \tilde{\delta} l_i^{t,h} D q_i^t = \sum_{j\in\Theta(i)} Q_{ij}^{t,h} - \left(Q_{mi}^{t,h} - x_{mi}\ell_{mi}^{t,h}\right), \quad \forall i \in \mathcal{N}^+, \forall t, \forall h \tag{31}$$

$$v_i^{t,h} - v_j^{t,h} = 2\left(r_{ij}P_{ij}^{t,h} + x_{ij}Q_{ij}^{t,h}\right) - \left(r_{ij}^2 + x_{ij}^2\right)\ell_{ij}^{t,h} + \Delta v_{ij}^{t,h} \quad \forall (i,j) \in \mathcal{E}, \forall t, \forall h \tag{32}$$

$$\ell_{ij}^{t,h} = \frac{\left(P_{ij}^{t,h}\right)^2 + \left(Q_{ij}^{t,h}\right)^2}{v_i^{s,t}}, \quad \forall (i,j) \in \mathcal{E}, \forall t, \forall h \tag{33}$$

$$\underline{U}^2 \le v_i^{t,h} \le \overline{U}^2, \quad \forall i \in \mathcal{N}^+, \forall t, \forall h \tag{34}$$

$$0 \le \ell_{ij}^{t,h} \le \overline{I}^2 u_{ij}^t, \quad \forall (i,j) \in \mathcal{E}, \forall t, \forall h \tag{35}$$

$$\left|\Delta v_{ij}^{t,h}\right| \le \left(\overline{U}^2 - \underline{U}^2\right)\left(1 - u_{ij}^t\right), \quad \forall (i,j) \in \mathcal{E}, \forall t, \forall h \tag{36}$$

$$-\overline{p}_0 \le p_0^{t,h} = \sum_{j\in\Theta(0)} P_{0j}^{t,h} \le \overline{p}_0, \quad \forall t, \forall h \tag{37}$$

$$-\overline{q}_0 \le q_0^{t,h} = \sum_{j\in\Theta(0)} Q_{0j}^{t,h} \le \overline{q}_0, \quad \forall t, \forall h \tag{38}$$

$$\text{Eqs. } (1) - (12) \tag{39}$$

Note that the active and reactive components of nodal power generation are defined in (20) and (21). In (22)-(23), the active power output of RES is assumed to be fully utilized under the grid-connected operation, while its reactive power output can be adjusted following the range of power factor angles, i.e., $[\gamma_k^{\min}, \gamma_k^{\max}] = [\tan\theta_k^{\min}, \tan\theta_k^{\max}]$. The generation and reserve constraints of DFGs are presented in (24) and (25) respectively. The operation of ES is modeled as in (26)-(29). To capture the operation of seasonally reconfigurable network, a nonlinear branch flow model (BFM) [37] with recoverable angle relaxation is presented in (30)-(33). Let $j \in \Theta(i)$ and m index the children nodes and the (unique) parent node of node i, the nodal active/reactive power balance is required as in (30) and (31). The enforcement of Kirchhoff's Voltage Law (KVL) as in (32) and (33) is controlled by reconfiguration variables, i.e., u_{ij}^t. When $u_{ij}^t = 0$, (32) is relaxed because of the auxiliary variable $\Delta v_{ij}^{t,h}$ in (36) [29], while the current and power flow variables are enforced to zero due to (33) and (35); Otherwise, constraints (32) and (33) are activated. The squared magnitudes of voltage and current are constrained by (34) and (35). The exchanged active/reactive power at substation node are constrained by (37) and (38), and the square of reference voltage level is fixed to a constant U_0^2. Finally, the seasonal G-MRC decisions are constrained by (1)-(12) as in (39).

Furthermore, the nonconvex equality (33) can be convexified by relaxing into a set of conic constraints [38]:

$$v_i^{t,h}\ell_{ij}^{t,h} \ge \left(P_{ij}^{t,h}\right)^2 + \left(Q_{ij}^{t,h}\right)^2, \quad \forall (i,j) \in \mathcal{E}, \forall t, \forall h \tag{40}$$

Note that (30)-(32) and (40) yields a convex SOCP approximation to the AC power flow model in (30)-(33), which could be exact under specific conditions as summarized in [38].

B. 2nd-Stage Problem: Validation of Reconfiguration and Reorganization Decisions Under On-Emergency Operation

Once encountering the extreme events, the ADN will transit from normal operation to on-emergency mode, which drives the networked system to be partitioned and disconnected from the utility grid. In such cases, each microgrid should be self-energized to immunize the uncertainties (i.e., the seasonal fluctuation of RES generation and load). Hence, in the second-stage, the feasibility of G-MRC decisions for emergency islandings will be checked under a finite set of scenarios $\omega \in \Omega$. A minimum energy loss model is defined to represent our second-stage problem (under scenario $\omega \in \Omega$) as follows:

$$\begin{aligned} \min\ z_{\text{ioc}}^{\omega} = & \sum_{t\in T}\sum_{h\in H}\sum_{(i,j)\in\mathcal{E}} \hbar^t \vartheta r_{ij}\ell_{ij}^{t,h,\omega}\Delta_h \\ & + \sum_{t\in T}\sum_{h\in H}\sum_{i\in\Psi} \hbar^t \varphi g l_i^{t,h,\omega}\Delta_h \\ & + \sum_{t\in T}\sum_{h\in H}\sum_{i\in\mathcal{N}^+} \hbar^t\left(\xi^1 p l_i^{t,h,\omega} + \xi^2 q l_i^{t,h,\omega}\right)\Delta_h \end{aligned} \tag{41}$$

$$s.t.,\ g l_i^{t,h,\omega} = \sum_{k\in\text{res}}\left[\delta r_{k,i}^{t,h}(\omega)\left(\bar{C}_{k,i} + \bar{C}_{k,i}^0\right) - g_{k,i}^{t,h,\omega}\right], \quad \forall i \in \Psi, \forall t, \forall h \tag{42}$$

$$p l_i^{t,h,\omega}, q l_i^{t,h,\omega} \ge 0, \quad \forall i \in \mathcal{N}^+, \forall t, \forall h \tag{43}$$

$$0 \le g_{k,i}^{t,h,\omega} \le \delta r_{k,i}^{t,h}(\omega)\left(\bar{C}_{k,i} + \bar{C}_{k,i}^0\right), \quad \forall k \in \text{res}, \forall i \in \Psi, \forall t, \forall h \tag{44}$$

$$p_{g,i}^{t,h,\omega} - \left(\delta l_i^{t,h}(\omega) D p_i^t - p l_i^{t,h,\omega}\right) = \sum_{j\in\Theta(i)} P_{ij}^{t,h,\omega} - \left(P_{mi}^{t,h,\omega} - r_{mi}\ell_{mi}^{t,h,\omega}\right), \forall i \in \mathcal{N}^+, \forall t, \forall h \tag{45}$$

$$q_{g,i}^{t,h,\omega} - \left(\delta l_i^{t,h}(\omega) D q_i^t - q l_i^{t,h,\omega}\right) = \sum_{j\in\Theta(i)} Q_{ij}^{t,h,\omega} - \left(Q_{mi}^{t,h,\omega} - x_{mi}\ell_{mi}^{t,h,\omega}\right), \forall i \in \mathcal{N}^+, \forall t, \forall h \tag{46}$$

$$v_i^{t,h,\omega} = U_0^2, \quad \forall i \in \Psi, \forall t, \forall h \tag{47}$$

$$\ell_{ij}^{t,h,\omega} \le \bar{I}^2\left(u_{ij}^t - w_{ij}^t\right), \quad \forall (i,j) \in \mathcal{E}, \forall t, \forall h \tag{48}$$

$$\left|\Delta v_{ij}^{t,h,\omega}\right| \le \left(\overline{U}^2 - \underline{U}^2\right)\left(1 - u_{ij}^t + w_{ij}^t\right), \forall (i,j) \in \mathcal{E}, \forall t, \forall h \tag{49}$$

$$\Xi^{\omega}\{\ (20),\ (21),\ (23)-(29),\ (32),\ (34),\ (40)\} \tag{50}$$

The second-stage objective function is presented in (41). In our study, the general energy loss cost is defined as the summation of penalty costs for network loss, RES curtailment and load shedding incurred by islanded operation. Note that the RES curtailment (as constrained by (42)) and load shedding can only be activated in on-emergency mode as remedy strategies, which are penalized by large cost factors φ and ξ. The imposing of penalty factor allows the relaxation of upper bounds on load shedding, as in (43). In (44) and (45)-(46), the variability of RES output and load demand are represented by random variables $\delta r_{k,i}^{t,h}(\omega)$ and $\delta l_i^{t,h}(\omega)$ respectively under scenario ω. Correspondingly, the operational variables constrained by (20), (21), (23)-(29), (32), (34)-(36), and (40) are also redefined under each scenario ω, as shown in (47)-(50). Note that in (47), the nodes with DER integration are selected as the reference nodes for each islanded microgrid. In addition, the binary variable $u_{ij}^t - w_{ij}^t$ is introduced in (48) and (49) to control the preventive G-MRC decisions for extreme events.

C. CVaR-Based Planning Reformulation

The influence of uncertain factors may increase the energy loss risk under emergency islandings. A popular way of risk management is resorting to the value-at-risk (VaR), i.e., a lower ϵ-quantile of the loss distribution [39], [40]. Note that the VaR measure is indifferent to the extreme scenarios that exceed VaR, which, however, may lead to substantial energy loss. To address this challenge, we introduce CVaR in place of VaR to quantitatively control the risks of those very adversarial scenarios. In our study, the CVaR for islanding risks is defined as the conditional expectation of energy loss cost z_{ioc}^{ω} subject to $z_{\text{ioc}}^{\omega} \ge \text{VaR}_{\epsilon}$, where ϵ is the confidence level. The sampling approximation form of CVaR [39] is adopted as in (51).

$$\text{CVaR}_{\epsilon} = \text{VaR}_{\epsilon} + \frac{1}{1-\epsilon}\sum_{\omega\in\Omega}\pi_{\omega}\left[z_{\text{ioc}}^{\omega} - \text{VaR}_{\epsilon}\right]^{+} \tag{51}$$

where $[t]^+ = \max\{0, t\}$. By using (51), we reformulate the energy loss function in (41) as a CVaR-based objective function to penalize the first-stage decisions that may cause extremely heavy losses. Accordingly, a risk-averse reformulation of RMP model is developed based on (1)-(32), (34)-(40) and (41)-(50). The full matrix form of our RMP model is given as follows:

$$\textbf{RMP}: \ \min c^T x + d^T y_0 + \theta(\text{VaR}_{\epsilon} + \frac{1}{1-\epsilon}\sum_{\omega\in\Omega}\pi_{\omega}\eta_{\omega}) \tag{52}$$

$$s.t.\ \eta_{\omega} \ge \max\left\{0, q^T y_{\omega} - \text{VaR}_{\epsilon}\right\}, \quad \forall \omega \in \Omega \tag{53}$$

$$H_1 u + H_2 w + H_3 x + H_4 \rho \ge h \tag{54}$$

$$Ax \ge b \tag{55}$$

$$\tilde{R}x + Fu + Dy_0 = \tilde{r} \tag{56}$$

$$\|G_l y_0\|_2 \le g_l^T y_0, \quad \forall l \in \mathcal{L} \tag{57}$$

$$R_{\omega}x + K_2 u + K_3 w + S y_{\omega} = r_{\omega}, \quad \forall \omega \in \Omega \tag{58}$$

$$\|B_l y_{\omega}\|_2 \le s_l^T y_{\omega}, \quad \forall l \in \mathcal{L}_{\omega}, \forall \omega \in \Omega \tag{59}$$

$$u, w \in \{0,1\},\ x \in \mathbb{Z}_+,\ \text{VaR}_{\epsilon}, \rho, y_0, y_{\omega}, \eta_{\omega} \in \mathbb{R},\ \forall \omega \in \Omega \tag{60}$$

The objective function is abstracted in (52), where θ denotes the risk level factor that makes a trade-off between the cost-minimization and risk-averse objectives. The vectors x and (u, w) represent the discrete decision variables of capacity expansion and seasonal G-MRC, while y_0 and y_{ω} denote the operational decisions defined under the grid-connected and islanding modes respectively. The first-stage constraints are presented in (53)-(57). Eq. (53) is introduced to compute the CVaR measure. Eq. (54) stands for the reconfiguration and reorganization constraints as in (1)-(12), where ρ denotes the auxiliary variables appeared in (5)-(7) and (9)-(12). Eq. (55) is to restrict the investment decisions, corresponding to (16)-(19). The linear constraints of grid-connected operation, i.e., (20)-(32) and (34)-(38), are represented by (56). Eq. (57) stands for the conic constraints as in (40), where $l \in \mathcal{L}$ is to index such constraints. The second-stage constraints, i.e., the linear constraints (associated with random variables) and the conic constraints of islanded operation, are denoted by (58) and (59) respectively.

IV. Strong Conic Duality and Customized Benders Decomposition Method

The mixed integer SOCP formulation with stochastic scenarios in (52)-(60) could be computationally very challenging, which demands an efficient decomposition algorithm. Traditionally, strong duality-based Benders decomposition method is often adopted to handle the similar but simpler mixed integer linear counterpart. Nevertheless, the strong duality property does not hold in general for an SOCP formulation [41]. If such property fails, Benders decomposition is not an exact algorithm. Hence, we should first investigate the strong duality issue of our formulation, and then describe the customization of Benders decomposition for fast computation.

A. Conic AC OPF Model With the Strong Duality

Although the dual of an SOCP formulation has been utilized in the literature, e.g., [36], [42], it is suggested in [41] that the strong duality should be studied according to its specifications to ensure rigorousness. So, we consider the particular SOCP formulation defined in (41)-(50) (i.e., the SOCP relaxation of second-stage AC OPF problem) and study its duality issue, which supports our algorithm development.

Proposition 1: For a fixed first-stage discrete solution $(\hat{x}, \hat{u}, \hat{w})$, the SOCP formulation (41)-(50) of a fixed scenario ω has the strong duality if the upper bounds of load shedding variables can be relaxed.

Proof: Following Slater's Condition [41], the strong duality holds for an SOCP if either its primal problem or dual problem is bounded and strictly feasible. Clearly, the objective function (41) is bounded from below. So we only need to prove that (42)-(50) is strictly feasible under the proposed

condition. For brevity, subscripts t, h, ω are removed in our proof.

Denote the nodal power injections by auxiliary variables $\tilde{p}_i$ and $\tilde{q}_i$ such that

$$\tilde{p}_i = p_{g,i} + pl_i - \delta l_i Dp_i, \quad \forall i \in \mathcal{N}^+ \tag{61}$$

$$\tilde{q}_i = q_{g,i} + ql_i - \delta l_i Dq_i, \quad \forall i \in \mathcal{N}^+ \tag{62}$$

$$\tilde{p}_i \in \mathcal{S}_i^p, \ \tilde{q}_i \in \mathcal{S}_i^q, \quad \forall i \in \mathcal{N}^+ \tag{63}$$

where $\mathcal{S}_i^p$ and $\mathcal{S}_i^q$ are convex sets surrounded by affine constraints (42)-(44) and (50) with fixed first-stage solution. Note that these affine convex sets, which define the feasible space for single operational variables, will never be empty. Then, let $\overline{p}_i = \sup\{\mathcal{S}_i^p\}$, $\underline{p}_i = \inf\{\mathcal{S}_i^p\}$, $\overline{q}_i = \sup\{\mathcal{S}_i^q\}$ and $\underline{q}_i = \inf\{\mathcal{S}_i^q\}$, the SOCP formulation defined in (45)-(49) and (61)-(63) is actually equivalent to the **OPF-SOCP** in [41].

Since the DERs output is curtailable under islanded operation, $\underline{p}_i, \underline{q}_i \leq 0$ holds for all $i \in \mathcal{N}^+$. On the other hand, we have $\overline{p}_i, \overline{q}_i = +\infty$ for all $i \in \mathcal{N}^+$ if the upper bounds of pl_i and ql_i are relaxed. So it follows condition C1-(d) in [41], i.e., $\underline{p}_i \leq 0 < \overline{p}_i$, $\underline{q}_i \leq 0 < \overline{q}_i$, that the strict feasibility of (45)-(49) and (61)-(63) is ensured. Consequently, the strong duality of the original SOCP formulation (41)-(50) is guaranteed. ■

Then, we give the matrix form of SOCP formulation (41)-(50) and its dual problem.

$$\textbf{Primal}: J_\omega^{\mathrm{p}} = \min \ q^T y_\omega \tag{64}$$

$$s.t. \ Sy_\omega = r_\omega - R_\omega \hat{x} - K_2 \hat{u} - K_3 \hat{w} : \mu_\omega \tag{65}$$

$$\|B_l y_\omega\|_2 \leq s_l^T y_\omega, \ \forall l \in \mathcal{L}_\omega : \gamma_\omega, \sigma_\omega \tag{66}$$

$$y_\omega \in \mathbb{R} \tag{67}$$

$$\textbf{Dual}: J_\omega^{\mathrm{d}} = \max \ \mu_\omega^T \left(r_\omega - R_\omega \hat{x} - K_2 \hat{u} - K_3 \hat{w}\right) \tag{68}$$

$$s.t. \ S^T \mu_\omega + \sum_{l \in \mathcal{L}_\omega} \left(B_l^T \gamma_\omega^l + \sigma_\omega^l s_l\right) = q \tag{69}$$

$$\left\|\gamma_\omega^l\right\|_2 \leq \sigma_\omega^l, \quad \forall l \in \mathcal{L}_\omega \tag{70}$$

$$\mu_\omega, \gamma_\omega^l \in \mathbb{R}, \ \sigma_\omega^l \in \mathbb{R}_+, \quad \forall l \in \mathcal{L}_\omega \tag{71}$$

where μ_ω and $\gamma_\omega^l, \sigma_\omega^l$ for all $l \in \mathcal{L}_\omega$ are the dual variables of our SOCP second-stage problem. Note that the proof of Proposition 1 is independent of $(\hat{x}, \hat{u}, \hat{w})$ and ω. Hence, the next result follows easily for (64)-(71).

Corollary 1: For any given first-stage discrete solution $(\hat{x}, \hat{u}, \hat{w})$, the strong duality of (64)-(71) holds, i.e., $J_\omega^{\mathrm{p}} = J_\omega^{\mathrm{d}}$ for all $\omega \in \Omega$.

B. Customized Benders Decomposition Algorithm

Denote *LB* and *UB* as the lower and upper bounds respectively, and *j* as the iteration counter. By using the strong duality of SOCP formulations (64)-(71), the iterative algorithm of customized Benders decomposition is developed as follows:

I *Initialization:* Set $LB = -\infty$, $UB = +\infty$, $j = 0$, $OC_\omega^j = \emptyset$; Set the termination gap ε.

II *Iterative Steps:*

– *Step 1:* Compute the master problem $\mathbf{MP}_j$:

$$z = \min c^T x + d^T y_0 + \theta \left(\mathrm{VaR}_\epsilon + \frac{1}{1-\epsilon} \sum_{\omega \in \Omega} \pi_\omega \eta_\omega\right) \tag{72}$$

$$s.t. \ \eta_\omega \geq \psi_\omega - \mathrm{VaR}_\epsilon, \quad \forall \omega \in \Omega \tag{73}$$

$$\psi_\omega \geq \hat{\mu}_{\omega,i}^T (r_\omega - R_\omega x - K_2 u - K_3 w), \quad \forall \omega \in \Omega, \ i = 1, \ldots, j-1 \tag{74}$$

$$\text{Eqs. (54)} - \text{(57)} \tag{75}$$

$$u, w \in \{0,1\}, x \in \mathbb{Z}_+, \mathrm{VaR}_\epsilon \in \mathbb{R}, \eta_\omega, \psi_\omega \in \mathbb{R}_+, \forall \omega \in \Omega \tag{76}$$

- If $\mathbf{MP}_j$ is infeasible, terminate the algorithm and *report the infeasibility of the original RMP problem*;
- Otherwise, derive an optimal solution $(\hat{x}, \hat{u}, \hat{w}, \hat{y}_0)$ and objective value $\underline{z}_j$, then update $LB = \underline{z}_j$ and $j = j + 1$;

– *Step 2:* For $(\hat{x}, \hat{u}, \hat{w})$, compute the dual of subproblem, i.e., (68)-(71), for every scenario $\omega \in \Omega$; Get the solutions as $(\hat{\mu}_{\omega,j}, \hat{\gamma}_{\omega,j}^l, \hat{\sigma}_{\omega,j}^l)$ and generate the Benders optimality cuts $OC_{\omega,j}$ as in (74);

– *Step 3:* Evaluate the objective function (52) under the current solution $(\hat{x}, \hat{u}, \hat{w}, \hat{y}_0)$ and the solution of (64)-(67), record current value $\overline{z}_j$ and update $UB = \min\{UB, \overline{z}_j\}$;

III *Termination Criterion:* If $|\frac{UB-LB}{LB}| \leq \varepsilon$, converge to the solution corresponding to the best *UB* and terminate the iterative steps; Otherwise, $\mathbf{MP}_j \leftarrow \mathbf{MP}_{j-1} \bigcup_{\omega \in \Omega} OC_{\omega,j}$, then go back to Step 1.

In the following, we prove the convergence issue of our Benders decomposition algorithm.

Corollary 2: The aforementioned Benders Decomposition algorithm either reports infeasibility or converges to the optimal value in finite steps.

Proof: Note that it is sufficient to consider the most stringent case where ε=0. We first consider the detection of infeasibility. According to Corollary 1, the second stage operational SOCP problem is always feasible with a finite optimal value for every random scenario, regardless of $(\hat{x}, \hat{u}, \hat{w})$. Hence, it is clear that the original RMP is infeasible if and only if the master problem $\mathbf{MP}_j$ with $j = 0$ is infeasible. Consequently, the RMP's infeasibility issue can be detected easily at the beginning of the algorithm.

To prove the convergence in the general case where RMP is feasible, we let LB_j and UB_j to denote the lower and upper bounds obtained in *j*-th iteration for the purpose of explanation. We claim that whenever $UB_j > LB_j$, the master problem $\mathbf{MP}_{j+1}$ must produce a new optimal solution $(\hat{x}, \hat{u}, \hat{w})$ that have not been derived in any previous iterations. Actually, if this is not the case, let $\mathbf{MP}_k$ with $k \leq j$ be the master problem that produces the same optimal solution. Then, we have $UB_{j+1} \leq UB_j \leq UB_k \leq LB_{j+1}$ that leads to the termination of the algorithm. Note that the first two inequalities follow from the update strategy of the upper bound defined in Step 3, and the last inequality follows from the strong duality presented in Corollary 1 and constraint (74) defined with respect to optimal dual solutions in $\mathbf{MP}_{j+1}$. Therefore, together with the fact that the feasible set of (x, u, w) is a bounded discrete set that has a finite number of points, the convergence clearly can be achieved within finite steps. ■

V. Numerical Results

The proposed G-MRC strategy and planning approaches (i.e., risk-averse RMP model and customized Benders decomposition (CBD) method) are verified through two microgrids test systems based on IEEE 33-bus network [37]

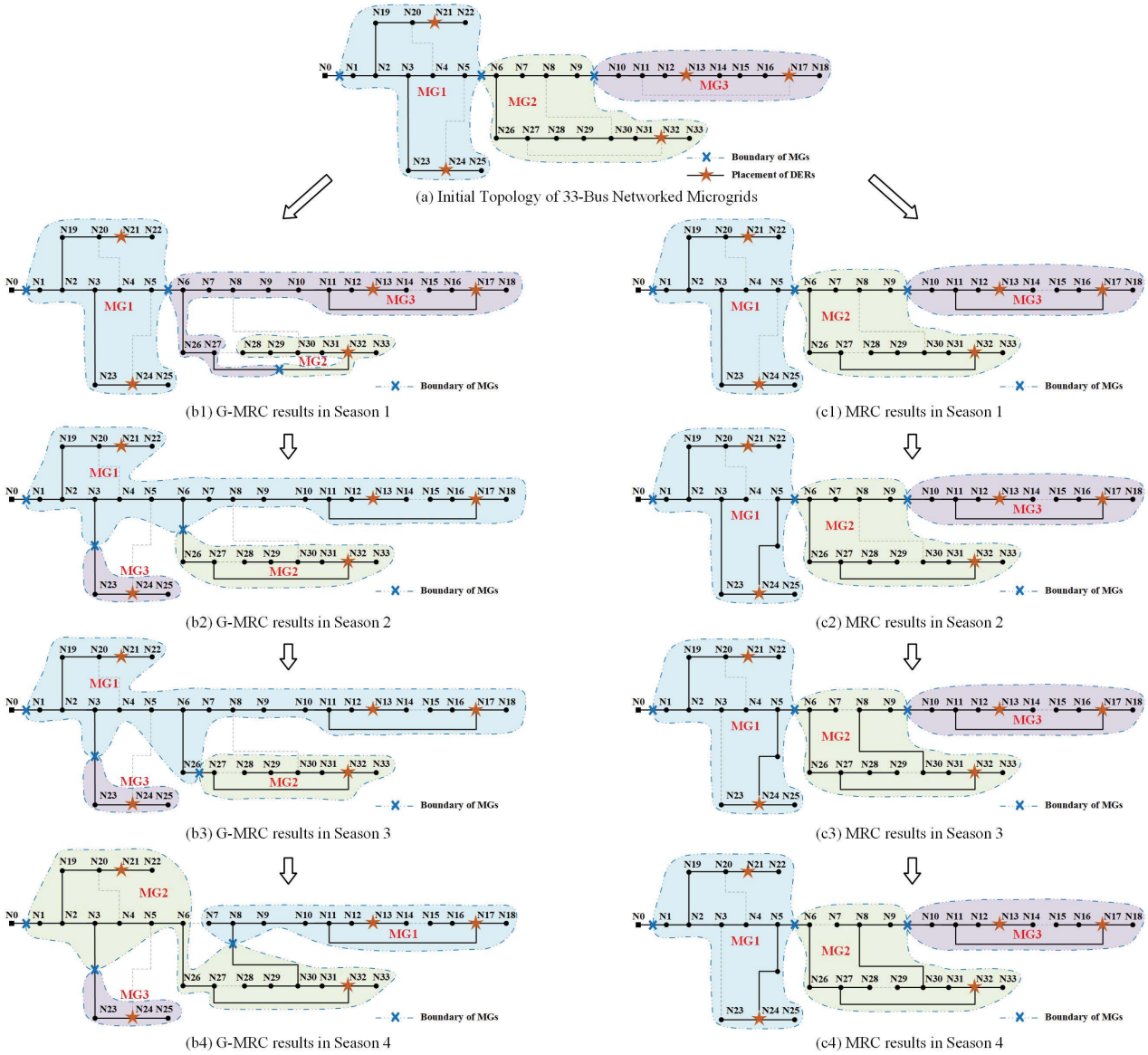

Fig. 2. Comparison of Generalized MRC with Traditional MRC for 33-Bus Networked Microgrids.

and SCE 56-bus network (a real-world distribution system served by Southern California Edison (SCE) Company [43]). Based on the standard systems, the demand growth is considered to be 20%, which drives the capacity expansion of DERs. The candidate facilities are chosen as solar panels (PVs), micro turbines (MTs), and battery banks (BBs) to represent RES, DFG, and ES respectively. To support our planning decision, 10,000 stochastic scenarios are sampled based on the empirical data of RES outputs and load profiles using the techniques mentioned in [44]. Besides, all the algorithm development and computations (including our CBD) are made by CPLEX in MATLAB environment on a PC with Intel Core i7-7820HQ 2.90GHZ processer and 32GB RAM.

A. 33-Bus Networked Microgrids

The initial topology of 33-bus networked microgrids is shown in Fig. 2(a), where the sectionalizing SSWs and tie SSWs are placed on solid and dashed lines respectively. 3 microgrids (MGs) are included with their boundaries (i.e., PCC points) denoted by "-X-", which are normally closed while opened under emergencies to form self-adequate islands. The initial settings of candidate DERs are listed in Table II [11], [23]. Other planning parameters can be referred to [44]. In this case, we first exhibit the seasonal G-MRC decisions and compare them with the traditional MRC schemes of the test network. Also, we derive the planning results via MRC and fixed network topology as benchmarks to validate the effectiveness of the proposed RMP model. In the aforementioned tests, 40 clustered stochastic scenarios are introduced to achieve a trade-off between the computational accuracy and efficiency. At last, the solution performance of CBD will be tested under an increasing number of scenarios.

1) Comparison of G-MRC With Traditional MRC: Fig. 2 presents the seasonal G-MRC and MRC (as the benchmark) decisions of 33-bus system. Note that both the G-MRC and MRC decisions are optimized in a global optimality manner.

TABLE II
INITIAL SETTINGS OF CANDIDATE DERS FOR 33-BUS SYSTEM

DER Type	PV	MT	BB
Major Parameters	Unit Cost: 1500$/kW $\cos\theta_k^{\min}$: -0.95 $\cos\theta_k^{\max}$: 0.95 Max Cap.: 2MW	Unit Cost: 300$/kW O&M Cost: 0.015$/kWh Fuel Cost: 0.139$/kWh Max Cap.: 1.2MW	Power Cost: 200$/kW Energy Cost: 150$/kWh O&M Cost: 0.001$/kWh Efficiency: 90% Max DOD: 90% Max Cap.: 1MW/2MWh
Placement & Initial Installation	N13(1MW), N21(0.72MW), N32(1.6MW)	N17(1MW), N24(0.72MW), N32(0.6MW)	N13(0.48MW/0.8MW), N21(0.48MW/0.8MW), N32(0.48MW/0.8MW)

TABLE III
RESULTS OF 33-BUS NETWORKED MICROGRIDS PLANNING VIA GENERALIZED MRC AND BENCHMARK STRATEGIES

Strategy	Capacity Expansion Plan					z_{inv} (k$)	z_{goc} (k$)	θCVaR (k$)	Total Cost(k$)	Cost Saving
	Node	PVs (MW)	MTs (MW)	BBs (MW)	BBs (MWh)					
Fixed Topo.	N13	0.04	0	0	0.02	760.4	1139.1	296.4	2196.0	/
	N17	0.25	0	0	0					
	N21	1.93	0.55	0.03	2.00					
	N24	1.40	0.07	0.01	0.04					
	N32	1.18	0.59	0	1.43					
MRC	N13	0	0	0	0	763.1	1075.8	248.0	2086.9	4.97%
	N17	0.50	0	0	0					
	N21	1.31	0.52	0	2.00					
	N24	1.87	0.10	0	0					
	N32	1.17	0.59	0	1.46					
G-MRC	N13	0	0.05	0	0.44	770.2	1070.1	206.5	2046.8	6.79%
	N17	1.64	0	0	0					
	N21	1.63	0.46	0	1.66					
	N24	1.56	0.10	0.16	0.87					
	N32	0.05	0.40	0	0.89					

As shown in Fig. 2(b1)-(b4), however, the involvement of dynamic boundaries facilitates the refinements of coverage areas, feeder configuration, and DERs allocation over the networked microgrids system. In contrast, as in Fig. 2(c1)-(c4), the traditional strategy is observed to reconfigure with the restriction of fixed microgrids boundaries. In the following, the differences between G-MRC and MRC are analyzed season by season:

- *Season 1:* The G-MRC is applied to the initial network through feeder reconfiguration and the relocation of PCC between MG2 and MG3. As a result, MG3 (with DER integration at N13 and N17) is expanded to supply more load nodes (i.e., N6-N9, N26-N27). Also, MG2 gains higher generation adequacy by shrinking its coverage area to N28-N33. In comparison, the MRC is conducted within the fixed boundaries of MG2 (by closing the SSW at L27-32 and opening the SSW at L27-28) and MG3 (by closing the SSW at L11-17 while opening the SSW at L14-15).
- *Season 2:* Based on the network in Season 1, the G-MRC is performed to reorganize the topology across all the microgrids. The new MG1 (i.e., N1-N22) is formed by merging the main bodies of MG1 and MG3, while a small part of MG1 is isolated to form the new MG3 (i.e., N23-N25). The rest load nodes are supplied by the new MG2 (i.e., N26-N33). Differently, the traditional scheme is to reconfigure MG1 (by closing the SSW at L5-24 and opening the SSW at L4-5) and MG2 (by closing the SSW at L27-28 while opening the SSW at L29-30).

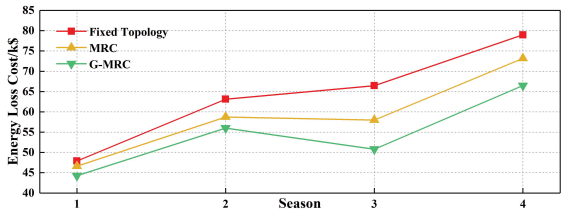

Fig. 3. Seasonal Varying Trend of Energy Loss Cost.

- *Season 3:* Based on the network in Season 2, the PCC that connects MG1 and MG2 is relocated from L6-26 to L26-27. In contrast, the traditional scheme is to reconfigure MG1 (by closing the SSW at L4-5 and opening the SSW at L3-23) and MG2 (by closing the SSW at L8-30 while opening the SSW at L7-8).
- *Season 4:* The G-MRC is conducted between MG1 and MG2. On one hand, MG1 shrinks to N7-N18 by opening the SSW at L6-7. On the other hand, MG2 is expanded by receiving the rest nodes (including the DER node N21) that once belonged to MG1. Then, the reorganized MG1 and MG2 are connected through a new PCC on L8-30. Differently, the MRC is only conducted in MG2 (by closing the SSW at L7-8 and opening the SSW at L6-7).

We notice that the effects of traditional reconfiguration strategy, which only change the topology of each microgrid within the fixed boundaries, are rather limited when comparing to G-MRC decisions. Hence, the dynamic reorganization of boundaries facilitates the networked microgrids to gain higher flexibility and adaptability.

2) Verification of Generalized Reconfiguration Strategy and Risk-Averse Planning Model: The G-MRC strategy as in Fig. 2(b1)-(b4) is then applied to support the capacity expansion planning of 33-bus networked microgrids. Table III presents the G-MRC based planning results given risk level $\theta = 0.60$ and confidence level $\epsilon = 90\%$. To validate the effectiveness of G-MRC, we set up two benchmark cases, i.e., microgrids planning with fixed topology and traditional MRC strategy, which are also provided in Table III. Note that the optimal values of investment cost (z_{inv}), operational cost (z_{goc}), and weighted CVaR cost (θCVaR) are evaluated as the performance metrics for planning solutions.

Comparing to the base case with fixed topology, the coordination of capacity expansion planning and G-MRC is observed to yield a slightly larger investment cost but much lower operational cost and weighted CVaR cost, and thus save the total cost by 6.79%. Also, the G-MRC based planning solution outperforms the MRC based one through a cost reduction of $40,113.9 (nearly 2%). It can be seen that the cost-saving is mostly achieved by reducing the energy loss under emergency islandings. Fig. 3 presents the seasonal varying trend of energy loss cost (ELC) under G-MRC and benchmark cases. Note that in the benchmarks, the emergency occasions could lead to a very large ELC especially in Season 3 and Season 4. However, the application of G-MRC has clearly reduced these costs, which implies a lower risk level for severe islanding scenarios under different seasons. Hence, comparing to those

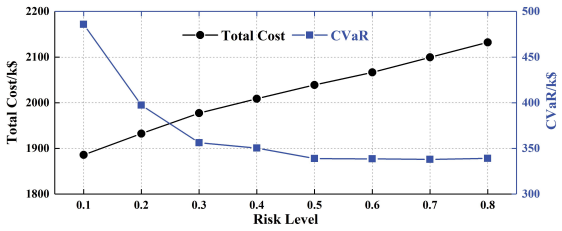

Fig. 4. Sensitivity Analysis of Risk-Control Parameter.

TABLE IV
COMPUTATIONAL TESTS OF CUSTOMIZED BENDERS DECOMPOSITION

N_s	CPX			CBD				Ratio of
	obj/k$	min	gap	obj/k$	itr	min	gap	Time Red.
4	1886.4	114.57		1887.8	10	8.61	0.08%	92.49%
8	1957.2	613.91		1958.3	10	10.14	0.31%	98.35%
20	/	T	N/A	2079.4	10	11.12	0.11%	/
40	/	O	N/A	2046.8	8	12.57	0.26%	/
80	/	O	N/A	2170.8	5	11.71	0.03%	/
120	/	O	N/A	2152.8	8	28.67	0.32%	/

fixed-boundaries schemes, the proposed strategy provides a reorganized microgrids topology with a superior performance, which could evidently improve the cost-efficiency of DERs investment as well as the operational feasibility of networked system especially under the on-emergency mode.

Furthermore, we investigate the impact of risk parameter θ on planning results. As shown in Fig. 4, by increasing the value of θ, the decision on RMP becomes more conservative with a lower CVaR and a larger total cost. It indicates that a larger θ could lead to a more costly planning solution but with a stronger risk-hedging capability. Certainly, when $\theta \geq 0.50$, the effect of risk reduction becomes marginal with the increase of risk level factor. These observations demonstrate the effectiveness of our risk-averse planning formulation, which provides a quantitative tool to control the risk level of G-MRC decisions.

3) Solution Performance of Customized Benders Decomposition Method: The computational feasibility of CBD is tested and compared with the direct use of CPLEX (CPX). The test results under different scenario numbers (N_s) are given in Table IV, where the objective values, iteration numbers, solution times (count in minutes), and remaining gaps are recorded in columns "obj", "itr", "min", and "gap", respectively. We set the gap threshold as 0.5% and the time limit as 720 mins. The solution time will be marked by "T" or "O" if any problem is running out of time or memory.

It can be seen that CBD successfully solves all the instances and performs much faster than CPX. With the increase of scenario number, we note that the solution capacity of CPX is limited up to an 8-scenario instance using 613.91 mins, while CBD spends only 10.14 mins (i.e., 98.35% time-saving compared to CPX) to address such a problem. For those can be solved by both methods, CBD attains similar results to CPX with a relative optimality gap less than 0.5% (which is reasonable due to our gap settings). For the instances involving more scenarios, CPX even fails to get any feasible solutions (with no gap information available) due to either the time limit or memory restriction. In contrast, our CBD spends less than 30 mins to address all these challenging instances (including an intractable 120-scenario instance). Hence, the direct solving of our mixed-integer SOCP formulation is proved to be very time-consuming even with a few scenarios. In comparison to CPX, however, the proposed algorithm can derive the planning solution with a similar precision but drastically reduce the computation time by orders of magnitude.

TABLE V
RESULTS OF 56-BUS NETWORKED MICROGRIDS PLANNING VIA GENERALIZED MRC AND BENCHMARK STRATEGIES

Strategy	Capacity Expansion Plan					z_{inv} (k$)	z_{goc} (k$)	θCVaR (k$)	Total Cost(k$)	Cost Saving
	Node	PVs (MW)	MTs (MW)	BBs (MW)	BBs (MWh)					
Fixed Topo.	N19	0.59	0.66	0.03	0	470.0	449.7	681.1	1600.8	/
	N21	2.00	0.59	0.30	1.48					
	N30	0	0.80	0.03	0.17					
	N45	0.63	0.80	0.84	2.00					
	N53	0.83	0.80	0	0					
MRC	N19	0.86	0.67	0	0	540.9	345.4	666.3	1552.6	3.01%
	N21	2.00	0.69	0.51	2.54					
	N30	0	0.44	0	0					
	N45	0.80	0.80	0.90	2.00					
	N53	0.84	0.77	0	0					
G-MRC	N19	1.18	0.59	0	0	570.4	341.0	290.9	1202.3	24.89%
	N21	2.00	0.80	1.30	3.20					
	N30	0.10	0.49	0	0					
	N45	0	0.56	1.00	2.00					
	N53	1.23	0.80	0	0					

B. 56-Bus Networked Microgrids

The proposed G-MRC strategy and planning methodology are further tested on a real-world 56-bus network. The detailed system data can be found in [43]. This network is originally equipped with 5MW PV generators at N45 and 0.6Mvar shunt capacitors for each of N19, N21, N30, and N53. These nodes are also selected as the candidate sites for DERs integration. Hence, the initial topology of 56-bus network is specified by including 4 microgrids, 5 candidate DER nodes, and 4 tie SSWs, as illustrated in Fig. 5(a). We note that most of these microgrids are not self-energized, which thus demand for capacity expansion and network reinforcement. Other parameter settings can be referred to Section V-A.

The seasonal G-MRC decisions for 56-bus network are presented in Fig. 5(b1)-(b4). The PCC that connects MG1 and MG3 is observed to be relocated along with the feeder reconfiguration in Season 1 and Season 4 to reorganize these microgrids. Through G-MRC, the DERs at node N21 (which originally belong to MG1) are transferred to supply MG3. Differently, as shown in Fig. 5(c1)-(c4), the traditional strategy only reconfigures each microgrid within the pre-determined domain. Also, Table V exhibits the planning solutions via G-MRC and two benchmark strategies. Comparing to the fixed-topology instance, the reinforcement through G-MRC has significantly reduced the total planning cost by nearly 25%. In contrast, the MRC based solution attains a much less cost-saving by only 3.01%. Moreover, the results of benchmark cases demonstrate that the improper island partitioning could lead to a very large risk penalty. By imposing the

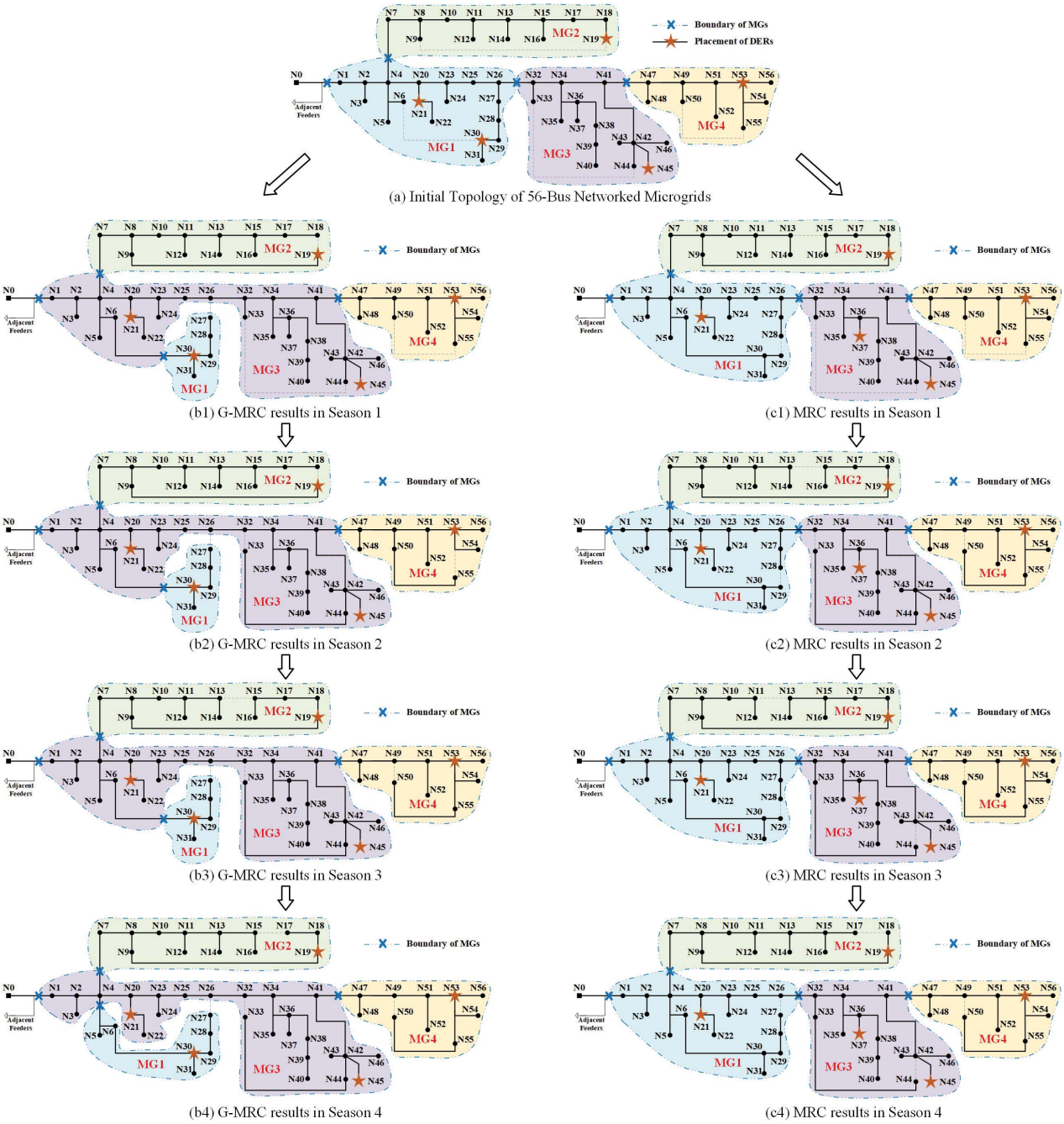

Fig. 5. Comparison of Generalized MRC with Traditional MRC for 56-Bus Networked Microgrids.

dynamic-boundary strategy, however, the CVaR cost is reduced from \$666,358.4 to \$290,912.8, which indicates a tremendous reduction in energy loss risks. Together with our observations in Section V-A, we can conclude that the proposed strategy extends the traditional concept of topology reconfiguration and fits well for networked microgrids.

VI. Conclusion

This paper presents a generalized network reconfiguration strategy to tackle the emergency islandings of microgrids. With this new strategy, a CVaR based stochastic mixed-integer conic model is developed to support the microgrids expansion planning with network reconfiguration and reorganizations. Also, we customize a strong conic-duality based Benders decomposition method to handle the computational issues. Numerical results on 33-bus test network and a real-world 56-bus system show that G-MRC achieves a significant cost-saving up to 22.56% comparing to the traditional reconfiguration strategy (i.e., with fixed boundaries). Hence, the proposed strategy enables the microgrids capacity expansion with higher cost-efficiency and system performance under both the normal operation mode and emergency islandings. Moreover, the customized decomposition algorithm demonstrates a superior

solution capacity to the direct use of a commercial solver, which thus supports the real application of our reorganizable microgrids planning method.

REFERENCES

[1] Z. Li, M. Shahidehpour, F. Aminifar, A. Alabdulwahab, and Y. Al-Turki, "Networked microgrids for enhancing the power system resilience," *Proc. IEEE*, vol. 105, no. 7, pp. 1289–1310, Jul. 2017.

[2] Z. Wang and J. Wang, "Self-healing resilient distribution systems based on sectionalization into microgrids," *IEEE Trans. Power Syst.*, vol. 30, no. 6, pp. 3139–3149, Nov. 2015.

[3] C. Chen, J. Wang, F. Qiu, and D. Zhao, "Resilient distribution system by microgrids formation after natural disasters," *IEEE Trans. Smart Grid*, vol. 7, no. 2, pp. 958–966, Mar. 2016.

[4] Z. Wang, B. Chen, J. Wang, J. Kim, and M. M. Begovic, "Robust optimization based optimal DG placement in microgrids," *IEEE Trans. Smart Grid*, vol. 5, no. 5, pp. 2173–2182, Sep. 2014.

[5] H. Wang and J. Huang, "Cooperative planning of renewable generations for interconnected microgrids," *IEEE Trans. Smart Grid*, vol. 7, no. 5, pp. 2486–2496, Sep. 2016.

[6] L. Che, X. Zhang, M. Shahidehpour, A. Alabdulwahab, and Y. Al-Turki, "Optimal planning of loop-based microgrid topology," *IEEE Trans. Smart Grid*, vol. 8, no. 4, pp. 1771–1781, Jul. 2017.

[7] L. Che, X. Zhang, M. Shahidehpour, A. Alabdulwahab, and A. Abusorrah, "Optimal interconnection planning of community microgrids with renewable energy sources," *IEEE Trans. Smart Grid*, vol. 8, no. 3, pp. 1054–1063, May 2017.

[8] S. Mojtahedzadeh, S. Ravadanegh, and M.-R. Haghifam, "Optimal multiple microgrids based forming of greenfield distribution network under uncertainty," *IET Renew. Power Gener.*, vol. 11, no. 7, pp. 1059–1068, 2017.

[9] F. S. Gazijahani and J. Salehi, "Robust design of microgrids with reconfigurable topology under severe uncertainty," *IEEE Trans. Sustain. Energy*, vol. 9, no. 2, pp. 559–569, Apr. 2018.

[10] E. Hajipour, M. Bozorg, and M. Fotuhi-Firuzabad, "Stochastic capacity expansion planning of remote microgrids with wind farms and energy storage," *IEEE Trans. Sustain. Energy*, vol. 6, no. 2, pp. 491–498, Apr. 2015.

[11] X. Cao, J. Wang, and B. Zeng, "A chance constrained information-gap decision model for multi-period microgrid planning," *IEEE Trans. Power Syst.*, vol. 33, no. 3, pp. 2684–2695, May 2018.

[12] Z. Wang, Y. Chen, S. Mei, S. Huang, and Y. Xu, "Optimal expansion planning of isolated microgrid with renewable energy resources and controllable loads," *IET Renew. Power Gen.*, vol. 11, no. 7, pp. 931–940, 2017.

[13] I. Alsaidan, A. Khodaei, and W. Gao, "A comprehensive battery energy storage optimal sizing model for microgrid applications," *IEEE Trans. Power Syst.*, vol. 33, no. 4, pp. 3968–3980, Jul. 2018.

[14] F. S. Gazijahani and J. Salehi, "Stochastic multi-objective framework for optimal dynamic planning of interconnected microgrids," *IET Renew. Power Gener.*, vol. 11, no. 14, pp. 1749–1759, Dec. 2017.

[15] F. S. Gazijahani and J. Salehi, "Optimal bilevel model for stochastic risk-based planning of microgrids under uncertainty," *IEEE Trans. Ind. Informat.*, vol. 14, no. 7, pp. 3054–3064, Jul. 2018.

[16] X. Shen, M. Shahidehpour, S. Zhu, Y. Han, and J. Zheng, "Multi-stage planning of active distribution networks considering the co-optimization of operation strategies," *IEEE Trans. Smart Grid*, vol. 9, no. 2, pp. 1425–1433, Mar. 2018.

[17] S. D. Manshadi and M. E. Khodayar, "Expansion of autonomous microgrids in active distribution networks," *IEEE Trans. Smart Grid*, vol. 9, no. 3, pp. 1878–1888, May 2018.

[18] M. E. Baran and F. F. Wu, "Network reconfiguration in distribution systems for loss reduction and load balancing," *IEEE Trans. Power Del.*, vol. 4, no. 2, pp. 1401–1407, Apr. 1989.

[19] S. Civanlar, J. J. Grainger, H. Yin, and S. S. H. Lee, "Distribution feeder reconfiguration for loss reduction," *IEEE Trans. Power Del.*, vol. PWRD-3, no. 3, pp. 1217–1223, Jul. 1988.

[20] B. Venkatesh, R. Ranjan, and H. B. Gooi, "Optimal reconfiguration of radial distribution systems to maximize loadability," *IEEE Trans. Power Syst.*, vol. 19, no. 1, pp. 260–266, Feb. 2004.

[21] R. A. Jabr, R. Singh, and B. C. Pal, "Minimum loss network reconfiguration using mixed-integer convex programming," *IEEE Trans. Power Syst.*, vol. 27, no. 2, pp. 1106–1115, May 2012.

[22] M. Lavorato, J. F. Franco, M. J. Rider, and R. Romero, "Imposing radiality constraints in distribution system optimization problems," *IEEE Trans. Power Syst.*, vol. 27, no. 1, pp. 172–180, Feb. 2012.

[23] Z. Tian, W. Wu, B. Zhang, and A. Bose, "Mixed-integer second-order cone programing model for VAR optimisation and network reconfiguration in active distribution networks," *IET Gener. Transm. Distrib.*, vol. 10, no. 8, pp. 1938–1946, 2016.

[24] S. Huang, Q. Wu, L. Cheng, and Z. Liu, "Optimal reconfiguration-based dynamic tariff for congestion management and line loss reduction in distribution networks," *IEEE Trans. Smart Grid*, vol. 7, no. 3, pp. 1295–1303, May 2016.

[25] X. Chen, W. Wu, and B. Zhang, "Robust capacity assessment of distributed generation in unbalanced distribution networks incorporating ANM techniques," *IEEE Trans. Sustain. Energy*, vol. 9, no. 2, pp. 651–663, Apr. 2018.

[26] H. Nafisi, V. Farahani, H. A. Abyaneh, and M. Abedi, "Optimal daily scheduling of reconfiguration based on minimisation of the cost of energy losses and switching operations in microgrids," *IET Gener. Transm. Distrib.*, vol. 9, no. 6, pp. 513–522, 2015.

[27] E. Dall'Anese and G. B. Giannakis, "Risk-constrained microgrid reconfiguration using group sparsity," *IEEE Trans. Sustain. Energy*, vol. 5, no. 4, pp. 1415–1425, Oct. 2014.

[28] M. M. A. Abdelaziz, H. E. Farag, and E. F. El-Saadany, "Optimum reconfiguration of droop-controlled islanded microgrids," *IEEE Trans. Power Syst.*, vol. 31, no. 3, pp. 2144–2153, May 2016.

[29] A. Kavousi-Fard, A. Zare, and A. Khodaei, "Effective dynamic scheduling of reconfigurable microgrids," *IEEE Trans. Power Syst.*, vol. 33, no. 5, pp. 5519–5530, Sep. 2018.

[30] M. Dabbaghjamanesh, A. Kavousi-Fard, and S. Mehraeen, "Effective scheduling of reconfigurable microgrids with dynamic thermal line rating," *IEEE Trans. Ind. Electron.*, vol. 66, no. 2, pp. 1552–1564, Feb. 2019.

[31] F. Shariatzadeh, C. B. Vellaithurai, S. S. Biswas, R. Zamora, and A. K. Srivastava, "Real-time implementation of intelligent reconfiguration algorithm for microgrid," *IEEE Trans. Sustain. Energy*, vol. 5, no. 2, pp. 598–607, Apr. 2014.

[32] "DOE microgrid workshop report," Microgrid Exchange Group, San Diego, CA, USA, Rep., 2011.

[33] M. E. Nassar and M. M. A. Salama, "Adaptive self-adequate microgrids using dynamic boundaries," *IEEE Trans. Smart Grid*, vol. 7, no. 1, pp. 105–113, Jan. 2016.

[34] Y.-J. Kim, J. Wang, and X. Lu, "A framework for load service restoration using dynamic change in boundaries of advanced microgrids with synchronous-machine DGs," *IEEE Trans. Smart Grid*, vol. 9, no. 4, pp. 3676–3690, Jul. 2018.

[35] C. Lin, W. Wu, B. Zhang, B. Wang, W. Zheng, and Z. Li, "Decentralized reactive power optimization method for transmission and distribution networks accommodating large-scale DG integration," *IEEE Trans. Sustain. Energy*, vol. 8, no. 1, pp. 363–373, Jan. 2017.

[36] H. Haghighat and B. Zeng, "Stochastic and chance-constrained conic distribution system expansion planning using bilinear Benders decomposition," *IEEE Trans. Power Syst.*, vol. 33, no. 3, pp. 2696–2705, May 2018.

[37] M. E. Baran and F. F. Wu, "Optimal capacitor placement on radial distribution systems," *IEEE Trans. Power Del.*, vol. 4, no. 1, pp. 725–734, Jan. 1989.

[38] S. H. Low, "Convex relaxation of optimal power flow—Part I: Formulations and equivalence," *IEEE Trans. Control Netw. Syst.*, vol. 1, no. 1, pp. 15–27, Mar. 2014.

[39] R. T. Rockafellar and S. Uryasev, "Optimization of conditional value-at-risk," *J. Risk*, vol. 2, no. 3, pp. 21–42, 2000.

[40] S. Sarykalin, G. Serraino, and S. Uryasev, "Value-at-risk vs. conditional value-at-risk in risk management and optimization," in *Tutorials in Operations Research*. Catonsville, MD, USA: INFORMS, 2008, pp. 270–294.

[41] X. Cao, J. Wang, and B. Zeng, "A study on the strong duality of conic relaxation of AC optimal power flow in radial networks," Xi'an Jiaotong University, Xi'an, China, Rep. arXiv:1807.08785v1, 2018.

[42] X. Wu, A. J. Conejo, and N. Amjady, "Robust security constrained ACOPF via conic programming: Identifying the worst contingencies," *IEEE Trans. Power Syst.*, vol. 33, no. 6, pp. 5884–5891, Nov. 2018.

[43] L. Gan, N. Li, U. Topcu, and S. H. Low, "Exact convex relaxation of optimal power flow in radial networks," *IEEE Trans. Autom. Control*, vol. 60, no. 1, pp. 72–87, Jan. 2015.

[44] X. Cao, J. Wang, and B. Zeng, "Distributed generation planning guidance through feasibility and profit analysis," *IEEE Trans. Smart Grid*, vol. 9, no. 5, pp. 5473–5475, Sep. 2018.

Xiaoyu Cao received the B.S. degree in electrical engineering from North China Electric Power University, Baoding, China, in 2013, and the Ph.D. degree in electrical engineering from Xi'an Jiaotong University, Xi'an, China, in 2019.

He is currently a Lecturer with the Systems Engineering Institute, Xian Jiaotong University. His current research interests include microgrids planning and scheduling, stochastic mixed-integer program with applications in smart grid and cyber-physical energy systems.

Jianxue Wang (M'11–SM'18) received the B.S., M.S., and Ph.D. degrees in electrical engineering from Xi'an Jiaotong University, Xi'an, China, in 1999, 2002, and 2006, respectively.

He is currently a Professor with the School of Electrical Engineering, Xi'an Jiaotong University. His current research interests include microgrid planning and scheduling, power system planning and scheduling, and electricity market.

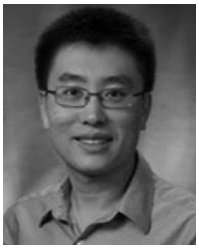

Jianhui Wang (M'07–SM'12) received the Ph.D. degree in electrical engineering from the Illinois Institute of Technology, Chicago, IL, USA, in 2007.

He had an eleven-year stint with Argonne National Laboratory with the last appointment as Section Lead—Advanced Grid Modeling. He is currently an Associate Professor with the Department of Electrical and Computer Engineering, Southern Methodist University, Dallas, TX, USA. He has held visiting positions in Europe, Australia, and Hong Kong, including a VELUX Visiting Professorship with the Technical University of Denmark. He was a recipient of the Highly Cited Researcher Award by Clarivate Analytics in 2018. He is the Secretary of the IEEE Power and Energy Society (PES) Power System Operations, Planning and Economics Committee. He is the Editor-in-Chief of the IEEE TRANSACTIONS ON SMART GRID and an IEEE PES Distinguished Lecturer.

Bo Zeng (M'11) received the Ph.D. degree in industrial engineering from Purdue University, West Lafayette, IN, USA, in 2007. He is currently an Associate Professor with the Department of Industrial Engineering and the Department of Electrical and Computer Engineering, University of Pittsburgh, Pittsburgh, PA, USA. His research interests include polyhedral study and algorithms for stochastic and robust mixed integer programs, coupled with applications in power and logistics systems. He is also a member of IISE and INFORMS.